



www.ijatir.org

Commutation Cell for Battery Charging using PV Panels in A Single Conversion Stage by using High-Voltage Gain Boost Converter

CHATRAGADDA PRIYANKA¹, M. LAKPATHI²

¹PG Scholar, Abdulkalam Institute of Technological Sciences, Kothagudem, Khammam, TS, India.

²Assistant Professor, Abdulkalam Institute of Technological Sciences, Kothagudem, Khammam, TS, India.

Abstract: This paper presents a novel high-voltage gain boost converter topology based on the three-state commutation cell for battery charging using PV panels and a reduced number of conversion stages. The presented converter operates in zero-voltage switching (ZVS) mode for all switches. By using the new concept of single-stage approaches, the converter can generate a dc bus with a battery bank or a photovoltaic panel array, allowing the simultaneous charge of the batteries according to the radiation level. The operation principle, design specifications, and experimental results from a 500-W prototype are presented in order to validate the proposed structure.

Keywords: Battery Chargers, DC–DC Power Conversion, Photovoltaic Power Systems.

I. INTRODUCTION

The increasing use of renewable energy in applications regarding distributed generation systems such as photovoltaic panels, fuel cells, and wind turbines leads power electronics researchers to new challenges. In this kind of application, one of the major concerns is the need of a high output dc-voltage bus (from 200 to 400 V_{dc}), which is necessary to supply inverters, UPS, etc., from low input voltage levels. This issue has led to the conception new several converter topologies. Nowadays, nonisolated dc–dc converters with high voltage gain have been highlighted in different applications. The traditional high-frequency isolated converters typically required a transformer responsible for processing the total rated power, with consequent increase of size, weight, and volume and reduction of efficiency. Converters with switched capacitors develop significant current peaks which limit the efficiency and the maximum processed power. A study on energy efficiency of switched-capacitor converters was present in, the authors presented some design rules useful for developing high-efficiency switched-capacitor converters, based on their analysis. In was presented several modular converter topologies based on a switched-capacitor cell concept, a soft-switched scheme was used in order to reduce the switching loss and electromagnetic interference.

A family of high-efficiency, high step-up dc–dc converters with simple topologies were proposed in. The proposed converters, use diodes and coupled windings instead of active switches to realize functions similar to those of active clamps, perform better than their active-clamp counterparts. The topology introduced in consists of an interleaved boost converter, where the inductor current ripple and the current stress through the main switches are reduced. Besides, reduction of volume, size, and weight is expected because the inductors are designed for twice the switching frequency. The converter presented in uses voltage multiplier cells that allow high voltage step-up with reduced stress regarding the semiconductor elements. The interleaved configuration allows the very reduction of the input inductors and the output capacitors, at the cost of high component count as additional multiplier cells are includes. A similar topology based on the three-state commutation cell was proposed in where the current sharing problem of the interleaved converter can be eliminated. The converter shown in presents a low input current ripple and uses an autotransformer with is designed for part of the rated power, while it is possible to achieve high voltage gain with reduced voltage stress across the switch. However, the use of such converter is limited to duty cycle value higher than 0.5.

II. DC-TO-DC CONVERTER

A DC-to-DC converter is an electronic circuit which converts a source of direct current (DC) from one voltage level to another. It is a class of power converter. DC to DC converters are important in portable electronic devices such as cellular phones and laptop computers, which are supplied with power from batteries primarily. Such electronic devices often contain several sub-circuits, each with its own voltage level requirement different from that supplied by the battery or an external supply (sometimes higher or lower than the supply voltage). Additionally, the battery voltage declines as its stored energy is drained. Switched DC to DC converters offer a method to increase voltage from a partially lowered battery voltage thereby saving space instead of using multiple batteries to accomplish the same thing. Most DC to DC converters also regulate the output voltage. Some exceptions include high-efficiency LED power sources, which are a kind of DC to DC converter that regulates the current through the LEDs, and simple charge pumps which double or triple the

output voltage. DC to DC converters developed to maximize the energy harvest for photovoltaic systems and for wind turbines are called power optimizers.

III. PHOTOVOLTAIC POWER SYSTEM

Photovoltaics (PV) is the name of a method of converting solar energy into direct current electricity using semiconducting materials that exhibit the photovoltaic effect, a phenomenon commonly studied in physics, photochemistry and electrochemistry. A photovoltaic system employs solar panels composed of a number of solar cells to supply usable solar power as shown in Fig.1. The process is both physical and chemical in nature, as the first step involves the photoelectric effect from which a second electrochemical process take place involving crystallized atoms being ionized in a series, generating an electric current. Power generation from solar PV has long been seen as a clean sustainable energy technology which draws upon the planet’s most plentiful and widely distributed renewable energy source – the sun. The direct conversion of sunlight to electricity occurs without any moving parts or environmental emissions during operation. It is well proven, as photovoltaic systems have now been used for fifty years in specialized applications, and grid-connected PV systems have been in use for over twenty years. They were first mass-produced in the year 2000, when German environmentalists including Eurosolar succeeded in obtaining government support for the 100,000 roofs program as shown in Fig.2.



Fig.1. Solar cells generate electricity directly from sunlight.



Fig.2. Photovoltaic SUDI shade is an autonomous and mobile station in France that provides energy for electric vehicles using solar energy.

IV. PROPOSED TOPOLOGY

A. Conception of the Topology

In the low voltage side, the bidirectional characteristic of the topology allows the MOSFET bridge to be supplied by either the battery or the PV array. Besides, the use of resonant capacitors in the full-bridge capacitors provides zero voltage switching (ZVS) of the switches. The integrated topology resulting from the boost converter and the three-state switching cell is shown in Fig. 3. The main advantage of this topology is the low voltage stress across the active switches, low input current ripple, and simplicity, what results in higher efficiency. Some high-voltage gain topologies are supposed to contain three dc links as shown in Fig. 4, where VDC3 feeds the inverter with a higher voltage than that of the remaining ones. According to the proposal, the battery bank and the photovoltaic panel can be connected to the low voltage side at VDC1 or VDC2, depending on the available voltage levels. Considering typical applications under 2 kW, battery bank voltage levels can be 12, 24, or 48 V (in order to avoid the connection of many units in series) and photovoltaic panels can be arranged to establish a dc link with voltage level equal to about twice that of the former link.

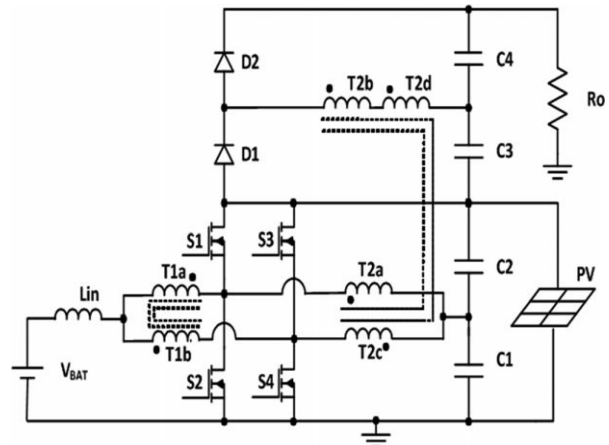


Fig.3. Proposed topology using a PV array.

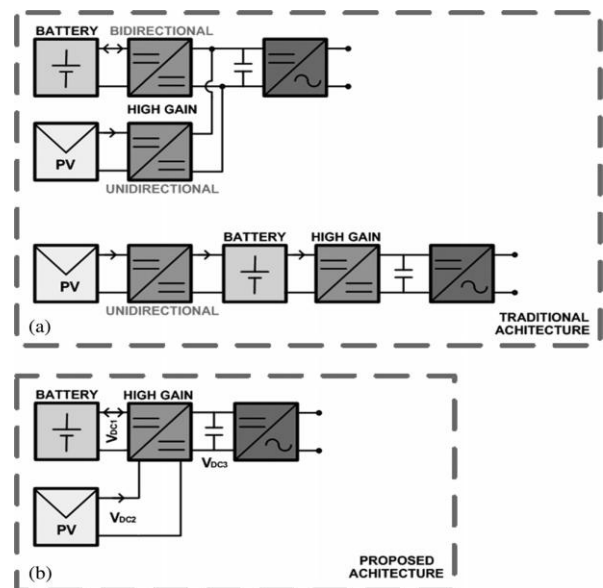


Fig.4.(a) Conventional Architecture. (b) Proposed Architecture.

Commutation Cell For Battery Charging using PV Panels in A Single Conversion Stage by using High-Voltage Gain Boost Converter

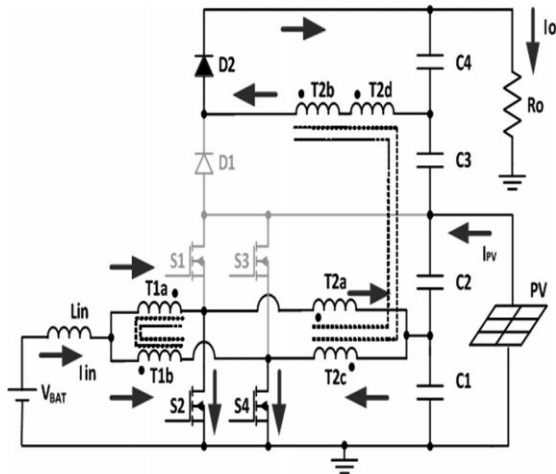


Fig. 5. First Stage.

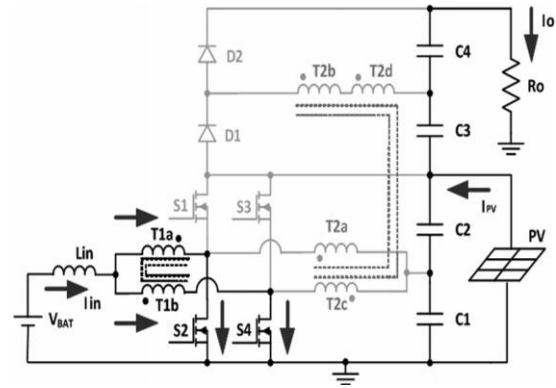


Fig. 9. Fifth Stage.

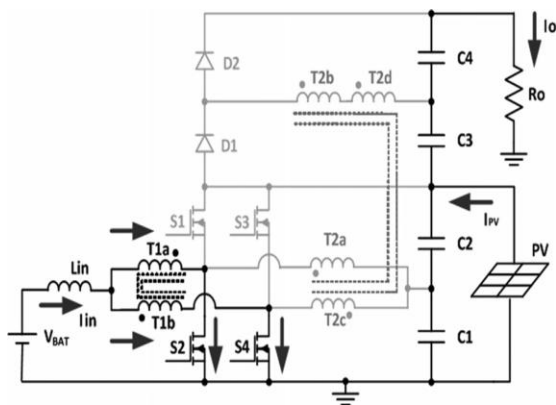


Fig. 6. Second Stage.

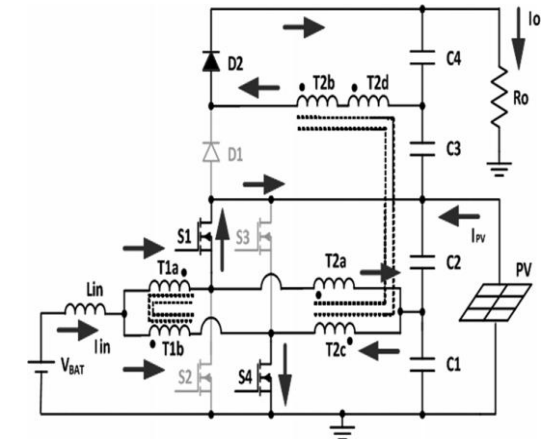


Fig. 10. Sixth Stage.

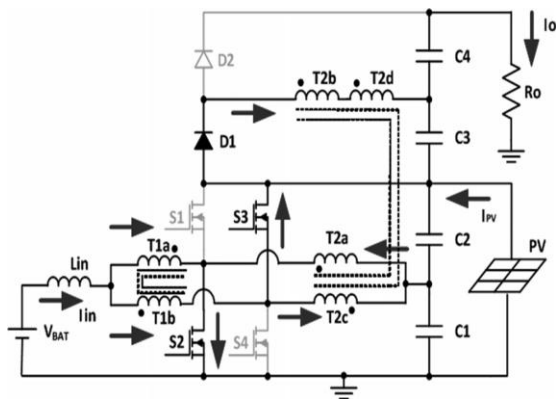


Fig. 7. Third Stage.

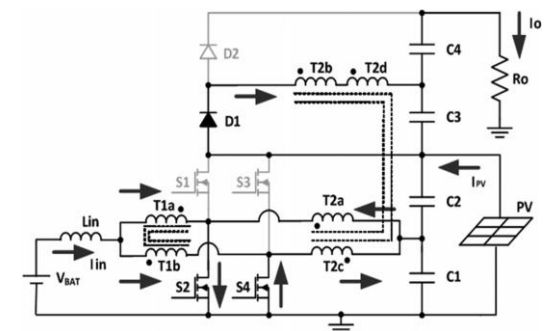


Fig. 8. Fourth Stage.

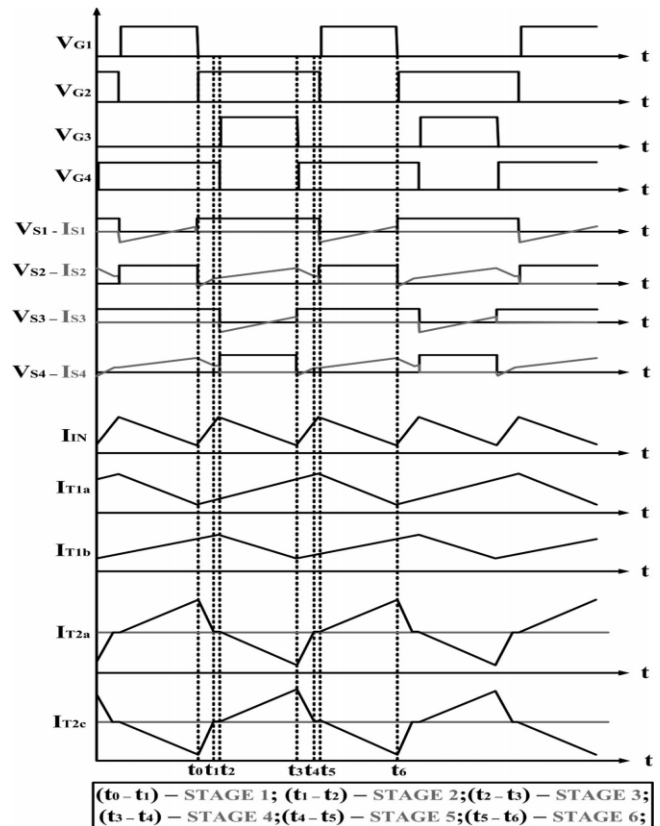


Fig. 11. Main theoretical waveforms.

The proposed topology is formed by one input inductor LIN, four controlled power switches S1–S4, two rectifier diodes D1 and D2, two transformers T1 (windings T1a and T1b) and T2 (windings T2a, T2b, T2c, and T2d) and four output capacitors C1–C4. Even though additional components are included, current sharing is maintained between (S1, S2, T1a, T2a) and (S3, S4, T1b, T2c). Then, besides the reduced current stress through the components, the instantaneous current during the turn OFF of the switches is significantly reduced for $D > 50\%$, thus leading to minimized switching losses. Also, the transformer is designed for about only 70% of the total output power. Within this context, it must be considered that there is no energy transfer from the input to the output during the second and fifth stages only. As a consequence, high efficiency is expected as shown in Figs.5 to 11.

B. Operation Principle

The proposed converter has two operation regions, which work analogously. The duty cycle is applied to the lower switches of each leg (S2 and S4), which operate in opposite phase. The converter behavior and the operation region are defined by the applied duty cycle. If the duty cycle is higher than 50%, the lower switches work in overlapping mode. However, if the duty cycle is lower than 50%, then only the upper switches are in an overlapping mode. As the operation principle regarding the switches is analogous, only the case for $D > 50\%$ is presented. The converter presents six operation stages, while Fig. 4. presents the theoretical waveforms. As it can be observed, the current through the input inductor has a frequency which is twice higher than the switching frequency, which characterizes the three-state commutation cell behavior. This current is then equally shared between the windings of the autotransformers, which leads to reduced current stresses. The windings T2a and T2c correspond to the transformer primary side, which are responsible for stepping the voltage up and allowing the switches to operate in the ZVS mode, increasing the system efficiency.

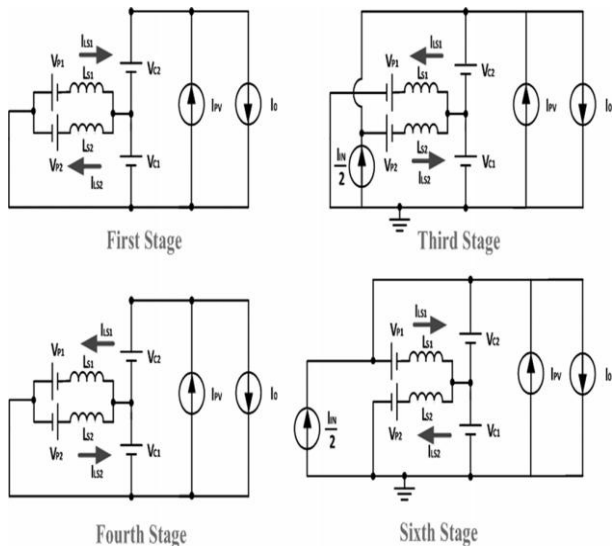


Fig.12. Equivalent circuits used to determinate static gain for $D > 50\%$.

First Stage [$t_0 - t_1$]: This stage begins when S1 is turned OFF, causing a current flow through the antiparallel diode of switch S2, allowing the turn ON in the ZVS mode. At this moment, S3 is turned OFF, and S4 is turned ON. The current flowing through the input inductor “IIN ” increases linearly and is equally divided between the two switching cells reducing the associated stresses of the active semiconductors. The current in the primary side T2a decreases linearly, while the current through T2c increases linearly. This stage ends when the currents in T2a and T2c reach zero, and the current through S2 is equal to that through S4.

Second Stage [$t_1 - t_2$]: Current “IIN ” still increases linearly and is equally divided through the commutation cells. Additionally, all the rectifier diodes are reverse biased. The current through T2a and T2c remains null. This stage ends when S4 is turned OFF.

Third Stage [$t_2 - t_3$]: This stage begins when S4 is turned OFF, causing the current to flow through the anti-parallel diode of S3, allowing the turn on in ZVS mode. At this moment, S2 is already turned on. The current flowing through the input inductor ‘IIN’ decreases linearly, while the currents through T1a and T1b increase and decrease linearly, respectively. The current in the primary side T2a decreases linearly, while the current through T2c increases linearly. This stage ends when S4 is turned ON and S3 is turned OFF.

Fourth Stage [$t_3 - t_4$]: This stage begins when S4 is turned ON. When S2 is turned ON, the input current “IIN ” increases linearly, and so do the currents through T1a and T1b. Also, the current through S4 increases and has flow in the opposite direction. The current through T2a linearly increases, while the one through T2c decreases. This stage ends when the currents in T2a and T2c reach zero, and the current through S2 is equal to the one in S4.

Fifth Stage [$t_4 - t_5$]: This stage is similar to the second one. In this stage, “IIN ” is still increasing linearly and is equally divided between the commutation cells. Besides, all the rectifier diodes are reverse biased. The current through T2a and T2c remain null. This stage ends when S2 is turned OFF.

Sixth Stage [$t_5 - t_6$]: This stage begins when S2 is turned OFF, causing a current flow through the antiparallel diode of S1, allowing its turn ON in the ZVS mode. At this moment, S3 is already turned OFF and S4 is turned ON. The current flowing through the input inductor “IIN ” decreases linearly. The current in the primary side T2a increases linearly, while the current through T2c decreases linearly. This stage ends when the currents through T2a and T2c become null, and the current through S2 is equal to the one through S4. After this stage, a new switching cycle begins from the first stage.

C. Static Gain

Considering that the duty cycle is applied to the lower switches, there are two possible operation modes. For $D > 50\%$, there is an overlapping period for the lower switches, which remain turned ON simultaneously during a certain time

Commutation Cell For Battery Charging using PV Panels in A Single Conversion Stage by using High-Voltage Gain Boost Converter

interval. On the other hand, for $D < 50\%$, there is an overlapping period of the upper switches.

Static Gain for $D > 50\%$: The equivalent circuits from which were derived equations are shown in Fig. 12. The output voltage can be obtained as

$$V_0 = V_{C1} + V_{C2} + V_{C3} + V_{C4} \quad (1)$$

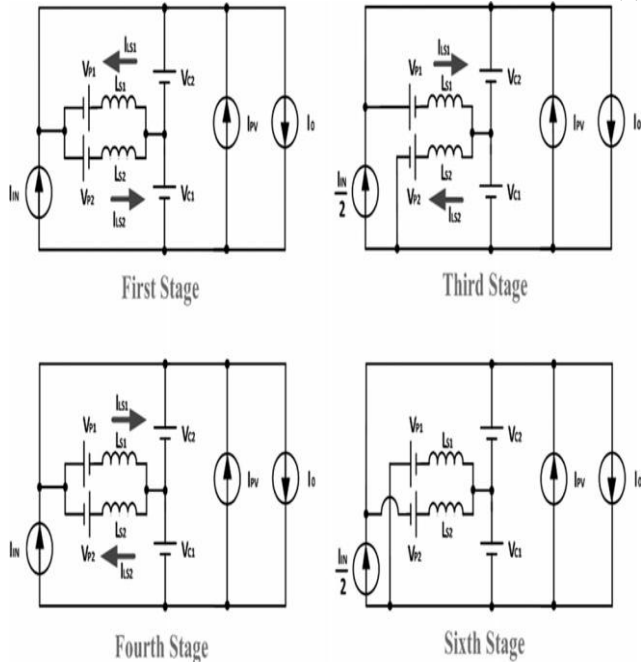


Fig.13. Equivalent circuits used to determinate static gain for $D < 50\%$.

Where

$$V_{C3} = V_{C4} = n \cdot (V_{P1} + V_{P2}) \quad (2)$$

V_{P1} and V_{P2} represent the transformer secondary voltage reflexed on primary side. Since the voltage across the capacitor C1 is equal to the voltage across the battery bank, V_{C1} and V_{C2} can be obtained as

$$\begin{aligned} V_{C1} &= V_{BAT} \\ V_{C2} &= \frac{D \cdot V_{BAT}}{1 - D} \end{aligned} \quad (3)$$

From the equations of the currents through the inductors L_{S1} and L_{S2} on the first stage (4), second stage (5), third stage (6) and from the time interval equations given in (7), the voltage across capacitors C3 and C4 can be obtained as (8)

$$\begin{cases} I_{LS1}(t) = I(0) - \left(\frac{V_{C1} + V_{P1}}{L_S}\right) \cdot t \\ I_{LS2}(t) = -I(0) + \left(\frac{V_{C1} - V_{P2}}{L_S}\right) \cdot t \end{cases} \quad (4)$$

$$\begin{cases} I_{LS1}(t) = I_{LS2}(t) = 0 \\ I_{LS1}(t) = \left(\frac{V_{C1} - V_{P1}}{L_S}\right) \cdot t \\ I_{LS2}(t) = \left(\frac{V_{C2} - V_{P2}}{L_S}\right) \cdot t \end{cases} \quad (5)$$

$$\begin{cases} \Delta t_1 = \Delta t_4 = \frac{[(1-D) \cdot T_s \cdot (n \cdot V_{C1} - V_{C4} + n \cdot V_{C2})]}{V_{C4}} \\ \Delta t_2 = \Delta t_5 = -\frac{[T_s \cdot (2 \cdot V_{C1} \cdot n \cdot (1-D) - V_{C4} + 2 \cdot V_{C2} \cdot n \cdot (1-D))]}{2 \cdot V_{C4}} \\ \Delta t_3 = \Delta t_6 = (1-D) \cdot T_s \end{cases} \quad (6)$$

$$V_{C3} = V_{C4} = \frac{n \cdot T_s \cdot V_{BAT}^2}{(1-D) \cdot T_s \cdot V_{BAT} + 4 \cdot I_0 \cdot L_S \cdot n} \quad (7)$$

From the previous equations, the static gain can be obtained as

$$G_{D>50\%} = \frac{V_0}{V_{BAT}} = \frac{1}{(1-D)} + \frac{2 \cdot n}{[(1-D) + \alpha]} \quad (8)$$

The static gain depends exclusively on the duty cycle “D,” the transformer turns ratio “n” and the normalized load current “ α .”

$$\alpha = \frac{4 \cdot n \cdot I_0 \cdot L_S}{V_{BAT} \cdot T_s} \quad (9)$$

Static Gain for $D \leq 50\%$: The equivalent circuits from which were derived equations are shown in Fig.13.

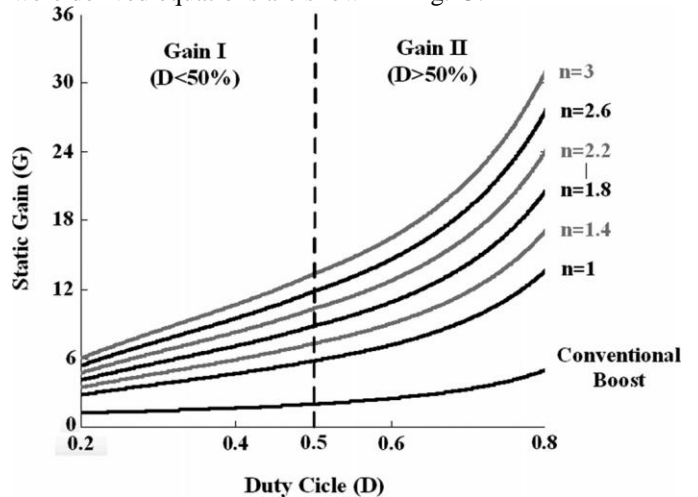


Fig. 14. G versus D for different values of ‘n’.

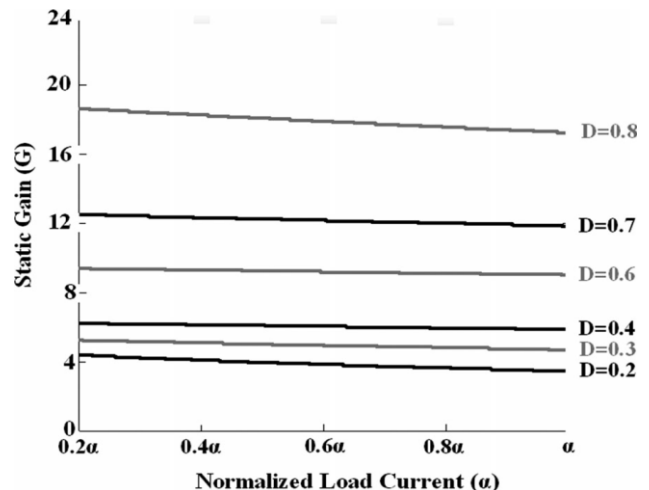


Fig.15. G versus D for different values of ‘D’.

The voltages across capacitors C1 and C2 are given by (2) and (3), but the voltages across capacitors C3 and C4 for $D < 50\%$ are given by

$$V_{C3} = V_{C4} = \frac{\left[2 \cdot I_0 \cdot n - \frac{D^2 \cdot T_s \cdot [V_{C3} \cdot (D-1) + n \cdot V_{C1}]^2}{2 \cdot L_s \cdot V_{C3} \cdot n \cdot (D-1)^2} \right] \cdot V_{C1}}{2 \cdot I_0 \cdot (1-D)} \quad (10)$$

Therefore, the static gain for $D < 50\%$ is given by

$$G_{D < 50\%} = \frac{V_0}{V_{BAT}} = \frac{1}{(1-D)} \cdot \left[\frac{2 \cdot n \cdot D^2}{D^2 + \alpha \cdot (1-D)} + 1 \right] \quad (11)$$

Fig. 14 presents the curves of the static gain G as a function of the duty cycle D for different values of n . Fig.15 presents the curves where the static gain G varied with the normalized load current α for different values of D .

D. Soft-Switching Condition

This section presents the analysis of minimum and maximum dead times necessary to obtain the soft-switching condition for the switches. In order to obtain soft switching, the leakage inductance of the transformer and the intrinsic capacitance of the switches are considered. Then, Fig. 16(a) presents the equivalent circuit during the turn OFF time of switch S1 and Fig.16(b) corresponds to the equivalent circuit during the turn OFF time of switch S2.

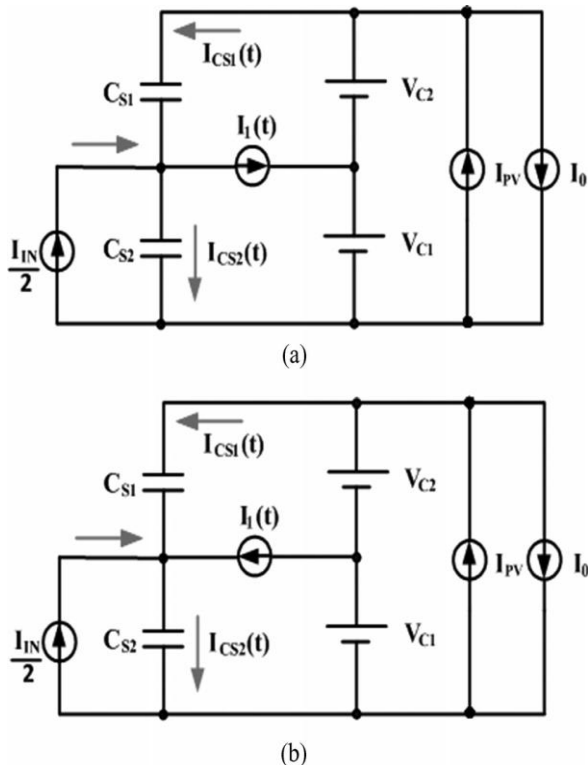


Fig. 16. Equivalent circuits used for the commutation analysis of topology III.

Considering the peak current value during stage 6 and the voltage across the primary winding V_{P1} in the first stage, the minimum dead time for the lower switches S2 and S4 can be obtained as

$$td_{MIN_S1NF} = \frac{\frac{I_{IN}}{2} - \left[\frac{\alpha \cdot D \cdot T_s}{2 \cdot L_s \cdot (D+\alpha)} \right] + \sqrt{\left(\frac{I_{IN}}{2} \right)^2 - 2 \cdot \frac{I_{IN}}{2} \cdot \left[\frac{\alpha \cdot D \cdot T_s}{2 \cdot L_s \cdot (D+\alpha)} \right] + \left[\frac{\alpha \cdot D \cdot T_s}{2 \cdot L_s \cdot (D+\alpha)} \right]^2}}{\sqrt{-4 \cdot C_s \cdot V_{PV} \cdot \left(\frac{D \cdot V_{PV}}{2 \cdot L_s \cdot (D+\alpha)} \right) - \frac{D \cdot V_{PV}}{2 \cdot L_s \cdot (D+\alpha)}}} \quad (12)$$

On the other hand, the maximum dead time that allows soft switching depends on the time interval necessary for the current to become zero during the first stage. Then the maximum dead time can be obtained as

$$td_{MAX_S1NF} = T_s \cdot \alpha - \frac{I_{IN} \cdot L_s \cdot (D + \alpha)}{D \cdot V_{PV}} \quad (13)$$

The commutation analysis for the upper switches can be performed analogously, while expression (15) can be easily derived and lower switches by varying with the normalized load current and for different values of duty cycle. From this figs.17 and 18, it can be observed that the duty cycle variation plays a small role in the commutation condition if compared with the switching interval.

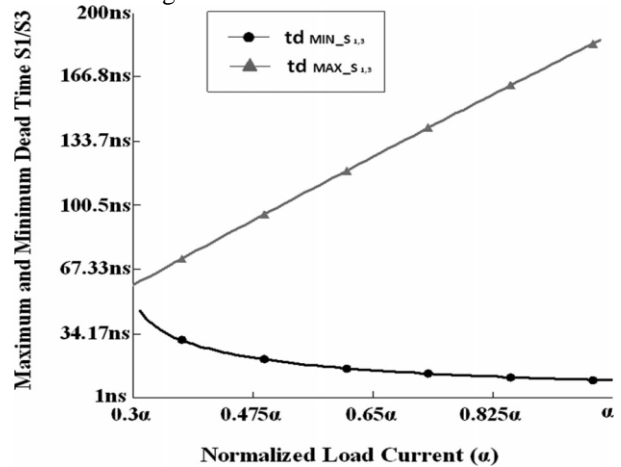


Fig.17. Soft-switching condition for the upper switches.

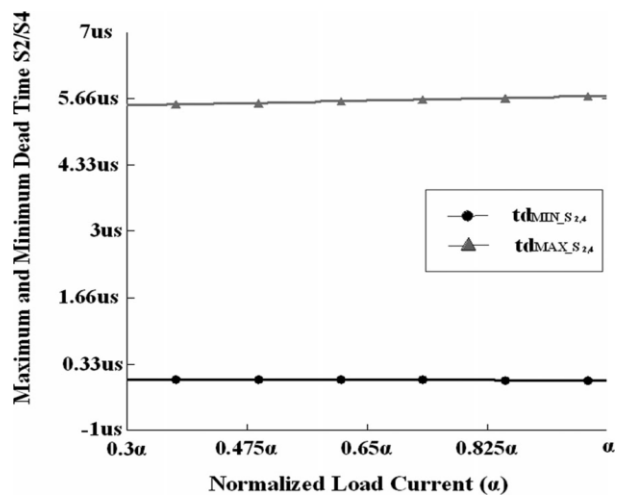


Fig.18. Soft-switching condition for the lower switches.

Commutation Cell For Battery Charging using PV Panels in A Single Conversion Stage by using High-Voltage Gain Boost Converter

$$td_{MAX_SUP} = \frac{\begin{bmatrix} (T_s \cdot V_{IN} \cdot \alpha) \\ -4 \cdot I_{PV} \cdot L_S \cdot n \\ + \frac{2 \cdot T_s \cdot V_{IN} \cdot n \cdot \alpha}{4 \cdot n \cdot (D-1)} \\ + \frac{T_s \cdot V_{IN} \cdot \alpha^2}{2 \cdot D \cdot (D+\alpha)} \end{bmatrix}}{V_{IN}^2 \cdot T_s \cdot \alpha} \quad (14)$$

E. Control Strategy

The strategy described in Fig.19 can be used in the proposed converter, where it is necessary to measure only three quantities that are the PV panel voltage V_{PV} , the PV panel current I_{PV} , and the voltage across the battery bank V_{BAT} . Let us suppose that constant power is supposed to be injected in the inverter stage. Considering that the battery has a low charge, the MPPT can be performed in any radiation and output power condition. The power difference is naturally transferred to or from the battery and the inverter can easily support the resulting dc-bus voltage variation. If the battery is fully charged, the MPPT is not performed and the operation point is changed until the current through the battery becomes zero.

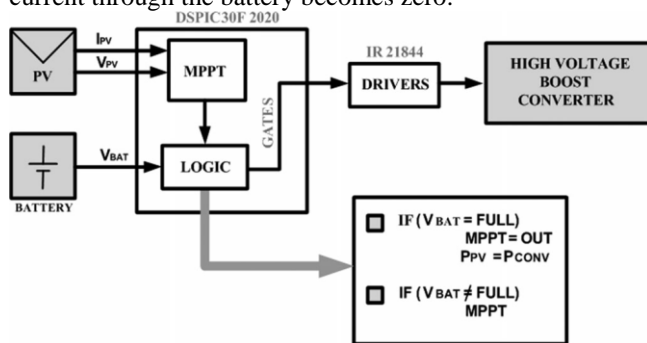


Fig. 19. Control strategy.

TABLE I: Prototype Specifications

Switching frequency	$f_s = 25 \text{ kHz}$
Input voltage	$V_{IN} = 24 \text{ V}$
Output voltage	$V_{out} = 200 \text{ V}$
Load power	$P_0 = 500 \text{ W}$
Input inductance	$L_{IN} = 100 \text{ uH}$
Leakage inductance	$L_K = 1 \text{ uH}$
Output capacitors	$C_1, C_2, C_3 \text{ and } C_4 = 100 \text{ uF}$
Turns ratio for the autotransformer of the three-state commutation cell	(1:1)
Transformer turns ratio	(1:1.4)
Switches	MOSFET IRFB4710
Diodes	MBR10200

V. SIMULATION AND RESULTS

This section presents the simulation results obtained from the converter operating in rated power condition. Table I shows the prototype specifications. Fig.20 presents the voltages across the output capacitors, where it can be seen that the sum of such quantities gives the output voltage. This result also shows good voltage sharing across the output capacitors. Fig. 22 presents the voltages across the diodes D1 and D2, which operate in complementarily way, while the voltages are clamped to approximately 150

V, i.e., there is no overvoltage. Fig. 22 presents the behavior of the input current and the currents through the switching cells, where good sharing exist between the currents through T1a and T1b. Consequently, the stresses regarding the active elements are reduced. Fig. 21 presents the voltage and the current through S1, where the operation ZVS mode is noticed. As it can be seen the conduction of the body diode can be avoided as S1 and S3 are used as synchronous rectifiers what reduce losses. Switch S3 presents the same behavior, although the waveforms are phase-shifted by 180° . Fig. 22 presents the voltage and the current through S2, whose operation is complementary to S1. It can be seen that S2 operates in the ZVS mode. Also, the current at the instant of the turning OFF is reduced what favors the turning OFF behavior.

Fig. 22 presents the open-loop converter dynamic behavior, where the bidirectional characteristic between the input voltage sources (batteries and photovoltaic panels) becomes evident. From such waveforms, one can be observe the behavior of the currents through the battery, the panel, and the load R_o , as well as the voltages across the panel and the load when a load step is performed.

A current step simulating the insertion of the photovoltaic panel is introduced at 45 ms, while the panel is responsible for supplying most of the energy and charging the batteries, since its current direction is inverted. Then, at approximately 55 ms, a load step of 50% is applied, where a small loss of the output voltage regulation characteristic can be observed. Fig. 22 presents the efficiency of the proposed converter, as well as the respective curves for topologies I and II, where it can be observed that higher efficiency is achieved in lower load condition (97%) and decreases in the rated condition (about 94%). This behavior can be explained since the transformers were designed for low core losses. Fig.21 presents the experimental prototype, where transformer T_r is split in two separate cores due to the availability of components.

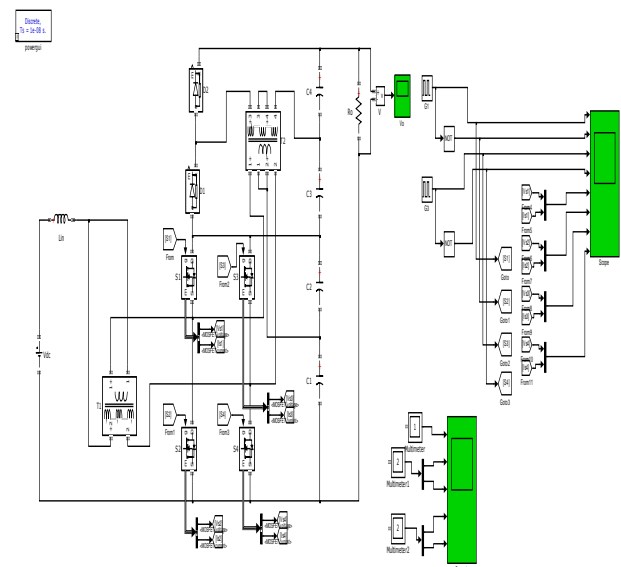


Fig.20. Simulation diagram.

VI. CONCLUSION

A boost converter with high voltage gain has been presented in this paper. The relevant equations for the design procedure, the operation principle, and the main theoretical waveforms are discussed in detail. The main advantage of the topology is the wide voltage step-up ratio with reduced voltage stress across the main switches, what is important in stand alone or in grid-connected systems based on battery storage, such as renewable energy systems. Simulation results obtained from a 500 W prototype have validated the concept, with high efficiency over a wide load range and smaller efficiency at the rated condition (94%), confirming the satisfactory performance of the structure. Although such curve is satisfactory for PV applications further optimization can be investigated in order to reduce conduction losses and improve efficiency in the rated condition. The concept of integrated converters in a single-stage approach seems to be promising, thus leading to the proposal of additional topologies feasible to photovoltaic and fuel cell applications.

VII. REFERENCES

[1] C. K. Cheung, S. C. Tan, C. K. Tse, and A. Ioinovici, "On energy efficiency of switched-capacitor converters," *IEEE Trans. Power Electron.*, vol. 28, no. 2, pp. 862–876, Feb. 2013.

[2] K. Zou, M. Scott, and J. Wang, "Switched-capacitor cell based voltage multipliers and dc-ac inverters," *IEEE Trans. Ind. Appl.*, vol. 48, no. 5, pp. 1598–1609, Sep./Oct. 2012.

[3] L. Wuhua, L. Xiaodong, D. Yan, L. Jun, and H. Xiangning, "A review of non-isolated high step-up DC/DC converters in renewable energy applications," in *Proc. 24th Annu. IEEE Appl. Power Electron. Conf. Expo.*, Feb. 15–19, 2009, pp. 364–369.

[4] D. S. Oliveira, Jr., R. P. T. Bascop'e, and C. E. A. Silva, "Proposal of a new high step-up converter for UPS applications," in *Proc. IEEE Int. Symp. Ind. Electron.*, 2006, vol. 2, pp. 1288–1292.

[5] S. M. Chen, T. J. Liang, L. S. Yang, and J. F. Chen, "A cascaded high stepup DC-DC converter with single switch for microsource applications," *IEEE Trans. Power Electron.*, vol. 26, no. 4, pp. 1146–1153, 2010.

[6] D. Jovicic, "Step-up DC-DC converter for megawatt size applications," *Power Electron., IET.*, vol. 2, no. 6, pp. 675–685, 2009.

[7] Y. Bo, L. Wuhua, W. Jiande, Z. Yi, and H. Xiangning, "A grid-connected PV power system with high step-up ZVT interleaved boost converter," in *Proc. 34th Annu. Conf. IEEE Ind. Electron.*, 2008, pp. 2082–2087.

[8] K. C. Tseng and T. J. Liang, "Novel high-efficiency step-up converter," *IEE Proc. Elect. Power Appl.*, vol. 151, no. 2, pp. 182–190, Mar. 2004.

[9] Z. Qun and F. C. Lee, "High-efficiency, high step-up DC-DC converters," *IEEE Trans. Power Electron.*, vol. 18, no. 1, pp. 65–73, Jan. 2003.

[10] G. A. L. Henn, R. N. A. L. Silva, P. P. Prac,a, L. H. S. C. Barreto, and D. S. Oliveira, "Interleaved-boost converter with high voltage gain," *IEEE Trans. Power Electron.*, vol. 25, no. 11, pp. 2753–2761, Nov. 2010.

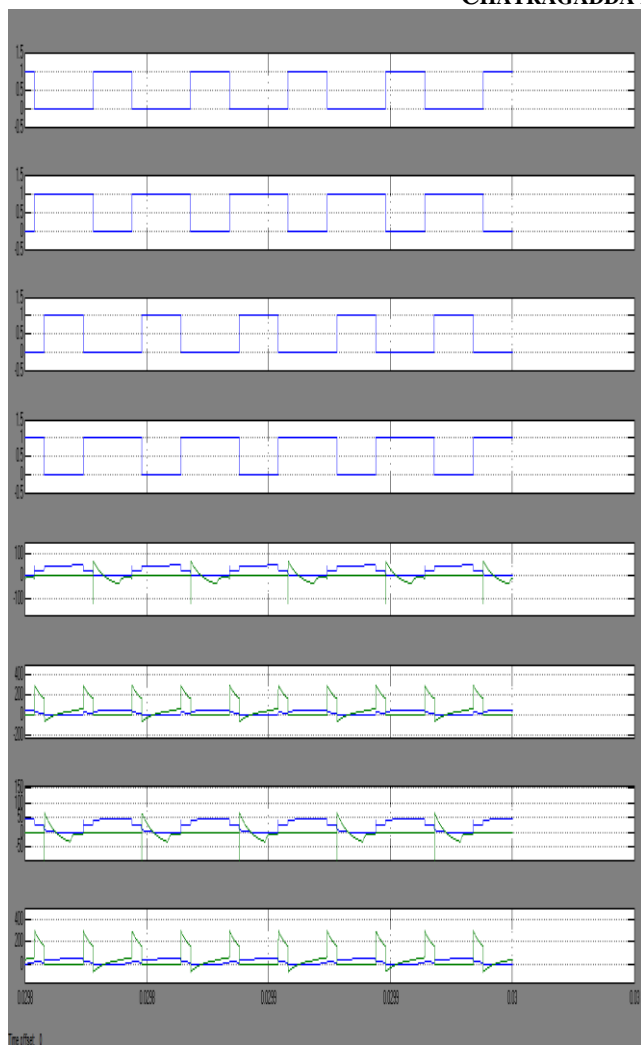


Fig.21. Voltage across the output capacitors.

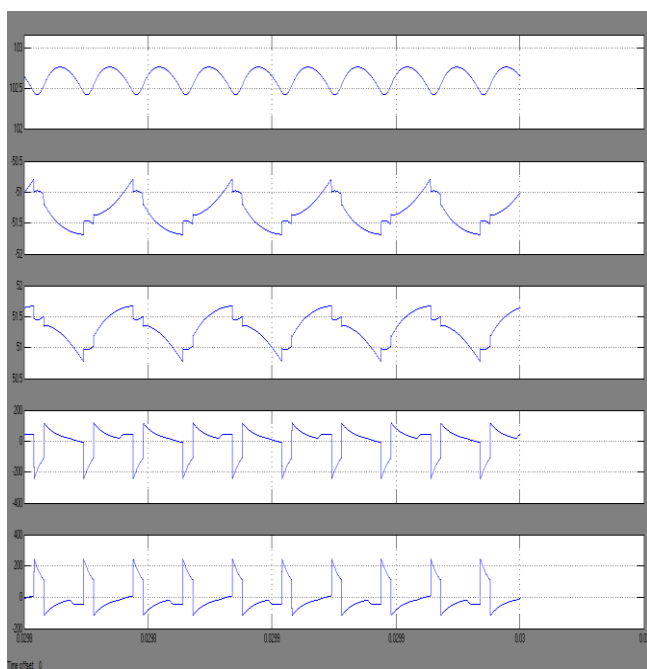


Fig.22. Input current and currents through the switching cells.

Commutation Cell For Battery Charging using PV Panels in A Single Conversion Stage by using High-Voltage Gain Boost Converter

Author's Profile:



Chatragadda Priyanka, received b.tech degree in Electrical and Electronics Engineering from Anubose Institute of Technology, Palvoncha, Khammam District, Telangana. And currently pursuing M.Tech in Electrical Power Systems at Abdulkalam Institute of Technological Sciences, Kothagudem, Khammam, T.S. My Areas of Interest Are Power Systems, and Power Electronics.



M.Lakpathi working as Assistant Professor in Abdulkalam Institute of Technological Sciences, Kothagudem, Khammam, Telangana, India. He Was Born In 1987 Aug,15. He Received The B.Tech Degree In Electrical & Electronics Engineering From S.R.R Engineering College, Karepally, Khammam, JNTUH, T.S, And He Received M.Tech. Degree in Electrical & Electronics Engineering as Power Electronics and Drives is Specialization from NIT Warangal, T.S. He Has A Teaching Experience of 4 Years. His Areas of Interest Are Power Electronics, Electrical Machines, Control Systems, Power Systems.